EVM, IM and Radiation Characteristics of a Bandwidth and Pattern Reconfigurable Antenna

Md. Asaduzzaman Towfiq, *Student, IEEE*, A. Khalat, Sebastián Blanch, Jordi Romeu, *Fellow, IEEE*, Lluís Jofre, *Fellow, IEEE*, and Bedri A. Cetiner, *Senior Member, IEEE*

***Abstract*—This paper presents the error vector magnitude (EVM), inter modulation (IM) and radiation performances of a reconfigurable antenna (RA) capable of varying its bandwidth between 3.4-3.6 GHz and 3.1-3.9 GHz bands, and steering its main beam into three directions pertaining to $\theta \in \{-30^\circ, 0^\circ, 30^\circ\}$, $\phi \in \{0^\circ\}$ for each band. The RA employs a multilayer structure, where two parasitically coupled reconfigurable layers using PIN diode switches enable generating the modes of operation. A fully functional RA has been fabricated and characterized. Maximum realized gain of $\sim$9 dB has been achieved for all modes of operation. Measurements indicated less than -25dB (5.6%) EVM for input powers up to 30dBm and revealed that the combined effects of loose solder joints and large non-linear response of PIN diodes are the main factors resulting in passive IM products.**

***Index Terms*—Reconfigurable antennas, Multifrequency antennas, EVM, PIM**

I. INTRODUCTION

The multilayer RA based on reconfigurable parasitic layer technique presented in this work is capable of performing both wide and narrow bandwidth operations. In addition, this RA can steer its main radiation beam towards three different directions for both bands. Combining bandwidth and pattern reconfigurability in a single compact platform provides advantages in effective sensing, transmission and frequency reuse [1]–[3].

Reflection coefficient and radiation pattern are most commonly used to characterize antennas. To determine the benefits of RAs used in a transceiver system requires characterizing the impacts that an RA plays on error vector magnitude(EVM) used as measure to quantify the performance of a transceiver. Also, signal distortion due to intermodulation (IM) products, whether it is passive IM (PIM) or is due to active elements, such as PIN diodes used in an RA, need to be measured. Although for traditional non-reconfigurable antennas some works investigated EVM [4], [5] and passive inter modulation (PIM) [6], [7], this has not been done for RAs. To that end, this work puts a great deal of efforts on characterizing the IM and EVM performances of the proposed RA. The main contributions of this work compared to related other works are, 1) concurrent configuration of impedance bandwidth and radiation pattern, 2) high realized gain ($\sim$9dB) for all modes , and 3) EVM and PIM investigations of the RA.

This work is supported in part by AFOSR Grant No FA 9550-15-1-0040DEF, DURIP Grant No: FA9550-16-1-0352

Md. A. Towfiq is with the i5 Technologies, Inc, Logan, Utah (e-mail: asaduzzaman.towfiq@i5technologies.com)

A. Khalat and B. Cetiner are with the Department of Electrical and Computer Engineering, Utah State University. (e-mails: khalat@aggiemail.usu.edu.,& bedri.cetiner@usu.edu.)

S. Blanch, L. Jofre, and J. Romeu are with the Department of Signal Theory and Communications, Universitat Politècnica de Catalunya, 08034 Barcelona, Spain (e-mails: {blanch,jofre,romeu}@tsc.upc.edu)

II. ANTENNA STRUCTURE AND RADIATION CHARACTERIZATION

The geometry of the RA and pixels interconnected by PIN diodes are shown in Fig. 1. The structure consists of four main layers, namely feed, driven antenna, parasitic patch and parasitic pixel layers. The working mechanism of this RA is based on well-established reconfigurable parasitic layer approach [8]. By connecting and disconnecting, the grid of 3×3 and 3×2 metallic pixels placed on the upper surfaces of the parasitic patch and pixel layers, respectively, and also controlling single PIN diode inserted in the microstrip feed line enables to achieve the reconfigurable modes of operations in terms of bandwidth and beam direction. The switches status and corresponding modes are given in Table I.

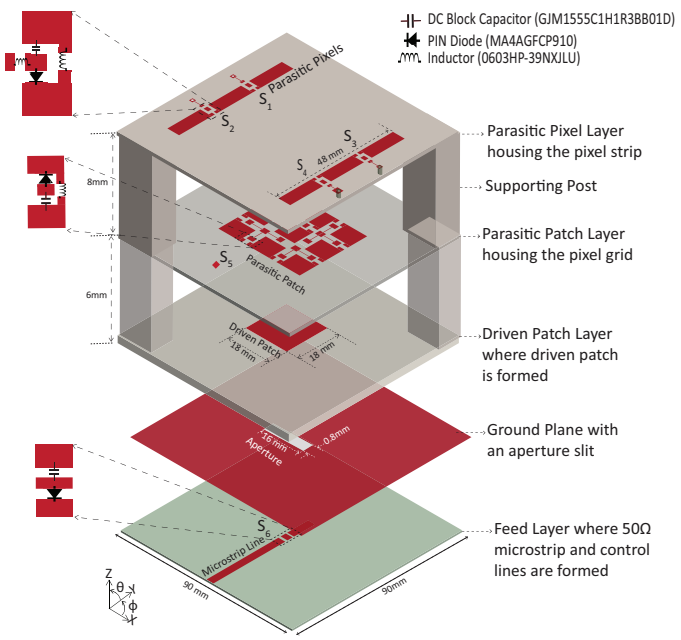

Fig. 1: 3D exploded view of the RA

A prototype RA was fabricated using standard printed circuit board fabrication processes and measured. PIN diode switches are numbered in Fig.1 as $S_i (i = 1 \ldots 6)$, where $S_i (i = 1, 2, 3, 4)$ are the switches integrated on parasitic pixel layer, S_5 represents the twelve switches used in parasitic

TABLE I: Switch Configurations and associated modes

Modes	θ	ϕ	BW(MHz)	S_1	S_2	S_3	S_4	S_5	S_6
1	0^o	0^o	200	0	0	0	0	0	1
2	30^o	0^o	200	0	0	1	1	0	1
3	-30^o	0^o	200	1	1	0	0	0	1
4	0^o	0^o	800	0	0	0	0	1	0
5	30^o	0^o	800	0	0	1	1	1	0
6	-30^o	0^o	800	1	1	0	0	1	0
11	N/A	N/A	N/A	0	0	0	0	0	0
22	N/A	N/A	N/A	0	0	1	1	0	0
33	N/A	N/A	N/A	1	1	0	0	0	0

patch layer, and S_6 is the switch integrated on microstrip feed line. The simulated and measured reflection coefficients and realized gain patterns for modes 1-6 are shown in Fig. 2 with good agreement between simulations and measurements. As predicted by simulations, the measured results show that modes 1,2 & 3 and modes 4,5 & 6 correspond to narrowband (3.4-3.6 GHz) and broadband (3.1-3.9 GHz) operations, respectively. The maximum realized gain is ∼9dB for all modes.

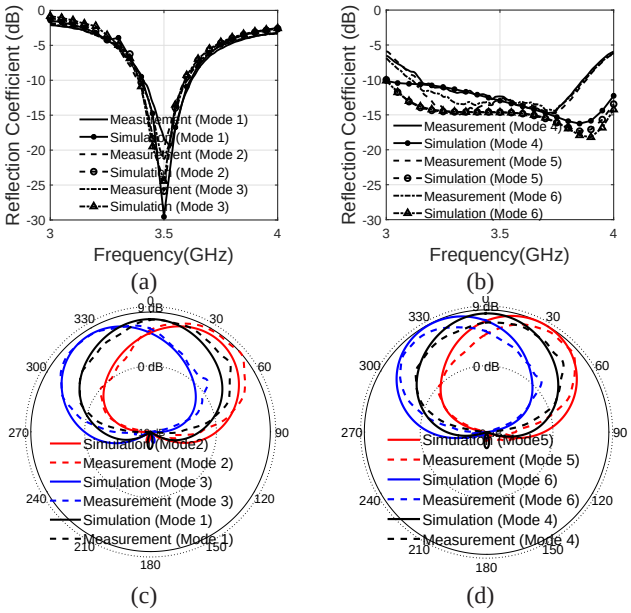

Fig. 2: Simulated and measured reflection coefficients of the RA for (a) mode 1,2, 3, (b) modes 4,5,6 and realized gain patterns at 3.5 GHz for (c) modes 1,2,3, and (d) modes 4,5,6

III. EVM AND PIM CHARACTERIZATION

A. EVM Characterization

EVM is commonly used to quantify the performance of a transceiver system, where the relative positions of the constellation points of an ideal case and non-ideal case considering non-ideal factors, are measured and compared. To determine the impact that the presented RA plays on EVM, a measurement set-up consisting of a vector signal generator (VSG) [9] and spectrum analyzer (SA) [10], as shown in Fig. 3(a) is used. In this set-up, VSG is used as a transmitter, where a quadrature amplitude modulation (QAM)-64 signal in the desired 3.5 GHz band is generated and is received by the SA. Only one modulation scheme is used as modulation scheme has little impact on EVM in either high or low distortion environment

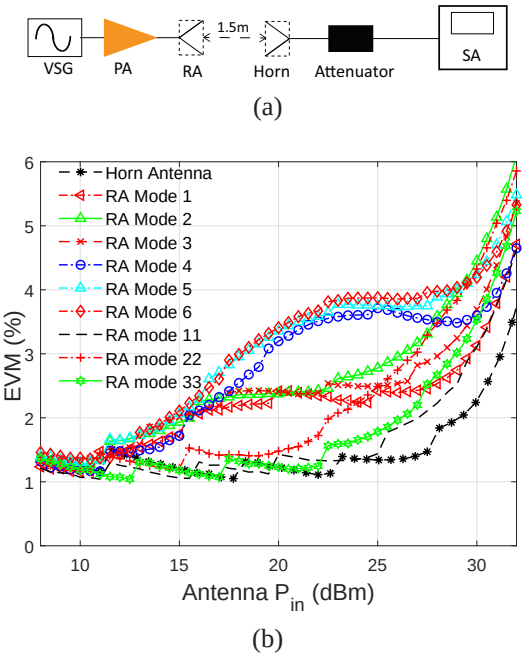

Fig. 3: (a) Schematic of the AUT measurement set-up and (b) measured EVM results for the RA modes and horn antenna, & extra RA modes (modes 11,22 &33) as a function of input power P_{in}

[11]. Before characterizing the EVM performance of the RA, the measurement setup was validated by performing two preliminary tests. In the first test, the VSG was directly connected to the SA, and EVM was measured as a function of input power (P_{in}). It was observed that the measured EVM is below -37dB (1.4%) for the range of P_{in}, -25dBm< P_{in} <0dBm. The degradation of the EVM corresponding to P_{in} <-25dBm is due to the reduction of signal to noise ratio (SNR), and for P_{in} >0dBm, there is a compression caused by the SA. Therefore, the measurement set-up was adjusted to provide the range of P_{in} values, -25dBm< P_{in} <0dBm, into the SA, which results in a 25dB measurement range and -37dB floor level. The second preliminary test was performed to assess the effect of the power amplifier (PA) [12] that was used in the RA measurements. This PA delivers upto 16W power with 47dB gain. Its 1-dB compression and 3^{rd}order intercept points are 39dBm and 47dBm, respectively. The result revealed that the PA does not have a significant impact in the degradation of the EVM for output powers (P_{out}) <25dBm. However, the non-linearities of the PA introduce a degradation for P_{out} >25dBm reducing the measurement range to 20dB for EVM <-37 dB.

As a reference, the EVM of a passive ridge-horn antenna was first measured, which also served to verify the setup. Measured results for different modes of the RA and for the horn are shown in Fig. 3(b). Some degradation in EVM corresponding to RA modes as compared to the EVM of the passive horn was observed. This degradation is due to the use of the PIN diode switches in RA.

The EVMs corresponding to the modes 4, 5, and 6, and to the modes 1, 2, and 3 exhibit similar behaviors, where the EVMs of modes 4, 5, and 6 are degraded slightly more than those of modes 1, 2, and 3. As shown in Table I, for modes 5

and 6, there are fourteen switches in ON state, with two being on the parasitic pixel layer and twelve being on the parasitic patch layer. For mode 4, there are twelve switches, which are all on the parasitic patch layer, in ON state. The EVMs of modes 5 and 6 are almost identical, where the EVM of mode 4 is slightly better. These results indicate that the impact of the two switches on the parasitic pixel layer is less as compared to the impact of the PIN diodes on the parasitic patch layer. The impact of the switches of patch layer being more is due to two main factors: (1) larger number of switches, i.e., twelve vs. four, and (2) the closer proximity of the parasitic patch layer with the driven patch layer. For modes 2 and 3, there are three switches (two on the parasitic pixel layer and one on the microstrip feed line) in ON state, while for mode 1, there is only one switch (on the microstrip feed line) in ON state. The EVM of mode 1 is slightly better than those of modes 2 and 3. These results also indicate that the impact of the switches of parasitic pixel layer is relatively less. However, the impact of the single switch on the microstrip feed line (S_6) is possibly larger than those of the parasitic pixel layer switches. To further investigate the impact of S_6, the EVMs of three additional modes have been measured. These modes and their corresponding switch statuses are given in Table I. Notice that these additional modes (modes 11, 22, and 33) have the same switch status with the modes 1, 2, and 3, except that S_6 is in OFF state. As seen from Fig. 3(b), the EVMs of modes 11, 22, and 33 are very close to that of a passive horn antenna. These results further indicate that the single switch on microstrip (S_6) plays a substantially larger role on the EVM performance than those of the four switches on the parasitic pixel layer.

The EVM characterization of the RA has revealed that the switch location in an RA architecture is as critical as the number of switches used. The impact of the interconnecting switch is increased when it is integrated into a region with increased RF signal strength. This is the case for S_6 integrated on the microstrip feed line. This also shows that the parasitic layer approach in RA design is an effective method as the degradation in EVM due to the switches integrated into parasitic pixel layer is negligible. It is worth noting that for $P_{in} > 25$dBm, the EVM measurements show the combined effect of the PA and the RA. Despite some degradation, for all six modes of operations, the EVM of the RA is less than -25dB (5.6%) for $P_{in} \leq 30$dBm, which is a good reference level for device validation purposes.

B. IM Characterization

Intermodulation (IM) products are generated due to the presence of nonlinearity, when a two-tone input signal of two closely spaced carriers at frequencies f_1 and f_2 feeds the antenna. The nonlinearity is either due to the use of nonlinear components such as PIN diodes or passive factors such as oxide layers that may exist between metal-to-metal contacts, electro-thermal effects, poor solder joints, and the use of ferromagnetic materials, i.e., nickel and steel. If IM products are located in the frequency band of interest, they cause interference with the desired signal resulting in distortion, which reduces receiver sensitivity. Also, it is worth noting that non-linear PIN diodes even unpowered or reverse biased and in the absence of PIM effects, may cause considerable non-linear distortions [13]–[15].

The IM characteristics of the presented RA were measured by using the set-up shown in Fig. 4. Two synthesizers [9] are used as sources to generate two carrier tones, where each individual tone is then amplified by a PA [12]. An isolator [16] is connected at the output of each PA to isolate them from the changes in the amplifier load conditions. The amplified carriers are combined by a combiner [17] and then fed to the RA through a directional coupler [18]. The directional coupler captures the signals reflected by the RA and channels them to SA [10], where the IM products are measured. A 20 dB attenuator is placed on the signal path going from the directional coupler to the spectrum analyzer so that the SA works within the adjusted optimum input power range (-25 dBm $< P_{in} <$ 0 dBm).

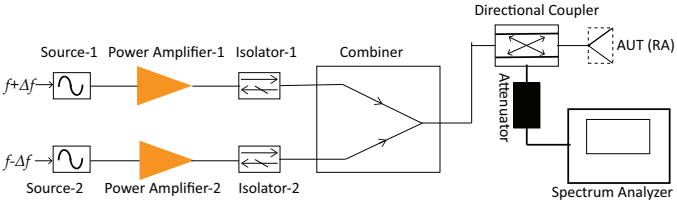

Fig. 4: PIM measurement setup

The sensitivity of the measurements, which is determined by the measurable lowest power value of the IM product, is limited by two factors. One is the noise floor of the SA, which depends on its noise figure and the resolution bandwidth of the measurement, which can be as low as 10 Hz. The second limiting factor is the IM product generation by the internal mixer of the SA itself. Notice in Fig. 4 that the reflected carriers by the RA are not filtered before going into the SA, thereby the two carriers plus the IM products generated by the RA are incident on the SA. Therefore, the internally generated IM products will also limit the sensitivity of the measurements. From the specifications of the SA [19], where the optimum incident power on the mixer (-35 dBm for 10 Hz resolution bandwidth) and the dynamic range (95 dB) are given, the sensitivity of our measurements is -130dBm.

At first, the measurement set-up has been calibrated at 3.5 GHz in terms of RF losses and power readings of the spectrum analyzer. To this end, the output powers of the synthesizers have been calibrated so that the individual signal power at carrier frequency incident on the RA is adjusted to 30 dBm. The source-1 and source-2 are set at 3.5GHz+$\frac{\triangle f}{2}$ and 3.5GHz-$\frac{\triangle f}{2}$, respectively, while the IM product is measured for the band, $3.5GHz - 1.5\triangle f \leqslant f \leqslant 3.5GHz + 1.5\triangle f$. The measured PIM revealed that the actual sensitivity of the measurement set-up is ∼-110 dBm. Fig. 5 shows the measured IM power in dBc (relative to carrier power) as a function of $\triangle f$ for different modes of the RA. The IM performance of a legacy patch antenna, which is obtained by removing the parasitic layers and the single PIN diode on microstrip feed line (S_6) of the RA, was also measured and used as a reference.

All the RA modes show relatively high IM power compared to the legacy patch antenna, which is expected due to the use of substantial number of switches in the multilayer RA.

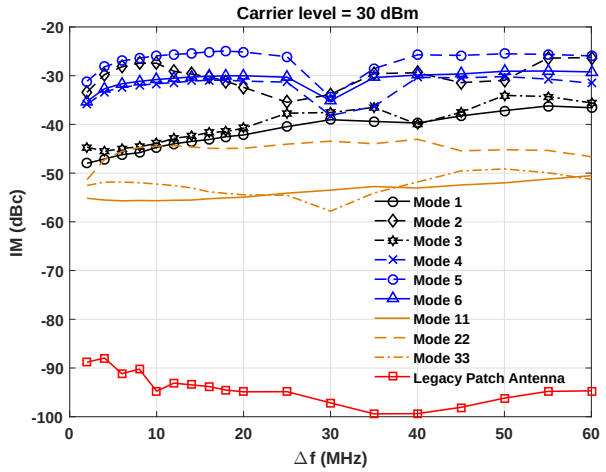

Fig. 5: PIM measurement results of the RA

Modes 4, 5 and 6 show the largest degradation in IM performance. While modes 4 and 6 show very similar behaviors with mode 4 performing slightly better, mode 5 has relatively higher IM power. As seen in Table I, these modes have the largest number of switches in ON state, where mode 4 uses twelve ON-state switches (all on parasitic patch layer), modes 5 and 6 use fourteen ON-state switches (two on parasitic pixel layer and twelve on parasitic patch layer). The small degradation in IM performance of mode 6 as compared to mode 4 is as expected and can be attributed to the two ON state switches of parasitic pixel layer (S_1 and S_2). Mode 5 for which the other two parasitic pixel layer switches (S_3 and S_4) are in ON state, exhibiting higher IM power than that of mode 6 is an indication that switches S_3 and S_4 may have loose solder joints. Nevertheless, these results indicate that the degradation in IM performance due to the parasitic pixel layer switches is smaller as compared to the switches on parasitic patch layer, which was the case for EVM performance as well.

The performances of modes 1, 2 and 3 are expected to be similar, as for these modes the numbers of switches in ON state are very close (one for mode 1 and three for modes 2 and 3). However, while modes 1 and 3 exhibit similar IM performances with mode 1 performing slightly better as expected, the performance of mode 2 is surprisingly poorer. As in the case of mode 5, this relatively high difference between modes 2 and 3 can be attributed to the poor solder joints of parasitic pixel layer switches of mode 2 (S_3 and S_4), which is known to substantially increase the PIM power due to electro-thermal effects. The difference between modes 1 and 3 being very small indicates that the impact of ON-state parasitic pixel layer switches (S_1 and S_2) on IM performance is smaller than that of the single switch on microstrip feed line.

To further investigate the individual roles that the interconnecting switches and parasitic layers play on the IM performance, three additional modes (modes 11, 22, and 33) were again measured. Mode 11 with all switches in OFF state shows the smallest IM power, which is ∼-55dBc, as expected. Mode 33 with S_1 and S_2 being in ON state show very similar behavior to that of mode 11. Mode 22 exhibiting unexpectedly higher IM power in comparison to modes 11 and 33 is similar to the behavior of mode 2 in comparison to modes 1 and 3. Approximately 40 dB difference observed between legacy patch (IM= ∼-95 dBc) and the RA with all switches in OFF state (mode 11 with IM = ∼-55 dBc) can be attributed to the combined effects of the passive factors such as loose solder joints and electro-thermal effects, and large non-linear response of PIN diodes even in unpowered or reverse biased condition. Around 30 dB difference observed in IM powers between the best mode (mode 11) and the worst mode (mode 5) is due to the combination of the activations of non-linear switches and aforementioned passive factors. Also, it is worth noting that the impact of an ON-state switch on PIM can be higher than that of an OFF-state switch, as the ON-state switch current increases the electro-thermal effects.

The IM powers of modes 1 & 3 are ∼15 dB larger than those of modes 11 & 33. As the only difference between these two set of modes is S_6 being in ON state for modes 1 & 3, this 15 dB degradation can be attributed to the operation of S_6. As in the case of EVM, S_6 integrated on the feed layer, which is exposed to relatively higher RF power, plays a significant role on IM performance as well. The IM powers of modes 4, 5, and 6 ($\sim$ -28 $<$ IM $<$ ∼-35 dBc) indicate that the parasitic pixel layer switches play a relatively smaller role as compared to the twelve switches of the parasitic patch layer on IM performance.

IV. Conclusion

Transceivers equipped with RAs require characterizing the RAs in terms of system level parameters such as error vector magnitude (EVM) and passive intermodulation product (PIM). The use of PIN diode switches in the presented RA causes small degradation in EVM performance as compared to passive horn antenna. For all six modes of operations, the measured EVMs were less than -25 dBm (5.6%) for an input power of 30 dBm. These results revealed that the roles that both the number of switches and their locations in RA structure play on EVM are equally important. The measured results for IM characterization reveal that the overall IM performance is contributed by the combined effects of the passive factors such as loose solder joints and electrothermal effects, and the inherit non-linear nature of PIN diodes. As the distortive effects on RA performance due to the inherit nonlinear nature of PIN diodes are unavoidable, it becomes important to minimize the effects resulting from non-linear passive factors such as loose solder joints and electro thermal effects. To this end, using effective multilayer printed circuit board manufacturing processes involving precise and high-yield pick/place procedures in mounting PIN diodes into the parasitic layers become critically important. The overall results showed that the parasitic pixel layer approach in implementing RAs is an effective approach as the degradation in EVM and PIM due to parasitic pixel layer switches is less as compared to the parasitic patch and microstrip feed layers with RF current distributions of higher magnitudes.

REFERENCES

[1] Z. Liu, K. Boyle, J. Krogerus, M. de Jongh, K. Reimann, R. Kaunisto, and J. Ollikainen, "Mems-switched, frequency-tunable hybrid slot/pifa antenna," *IEEE Antennas and Wireless Propagation Letters*, vol. 8, pp. 311–314, 2009.

[2] M. Hamid, P. Gardner, P. S. Hall, and F. Ghanem, "Switched-band vivaldi antenna," *IEEE transactions on antennas and propagation*, vol. 59, no. 5, pp. 1472–1480, 2011.

[3] B. Cetiner, H. Jafarkhani, J.-Y. Qian, H. J. Yoo, A. Grau, and F. De Flaviis, "Multifunctional reconfigurable MEMS integrated antennas for adaptive MIMO systems," *IEEE Communications Magazine*, vol. 42, no. 12, pp. 62–70, 2004.

[4] F. A. Miranda, C. H. Mueller, and M. A. B. Meador, "Aerogel antennas communications study using error vector magnitude measurements," in *2014 IEEE Antennas and Propagation Society International Symposium (APSURSI)*, July 2014, pp. 1149–1150.

[5] G. H. Huff, N. Soldner, W. D. Palmer, and J. T. Bernhard, "Study of error vector magnitude patterns (evrp) for a transmit/receive pair of microstrip patch antennas," in *2006 IEEE Antennas and Propagation Society International Symposium*, July 2006, pp. 449–452.

[6] J. R. Wilkerson, I. M. Kilgore, K. G. Gard, and M. B. Steer, "Passive intermodulation distortion in antennas," *IEEE Transactions on Antennas and Propagation*, vol. 63, no. 2, pp. 474–482, Feb 2015.

[7] D. Wu, Y. Xie, Y. Kuang, and L. Niu, "Prediction of passive intermodulation on mesh reflector antenna using collaborative simulation: Multi-scale equivalent method and nonlinear model," *IEEE Transactions on Antennas and Propagation*, vol. PP, no. 99, pp. 1–1, 2017.

[8] X. Yuan, Z. Li, D. Rodrigo, H. S. Mopidevi, O. Kaynar, L. Jofre, and B. A. Cetiner, "A parasitic layer-based reconfigurable antenna design by multi-objective optimization," *IEEE Transactions on Antennas and Propagation*, vol. 60, no. 6, pp. 2690–2701, June 2012.

[9] *SMA100A Vector Signal Generator*, RHODE&SCHWARTZ, option: FSL-k91.

[10] *FSL-6 Spectrum Analyzer*, RHODE&SCHWARTZ, option: FSL-k91.

[11] M. D. McKinley, K. A. Remley, M. Myslinski, J. S. Kenney, D. Schreurs, and B. Nauwelaers, "Evm calculation for broadband modulated signals," in *64th ARFTG Conf. Dig*, 2004, pp. 45–52.

[12] *ZHL-16w-43+ High Power Amplifier*, Minicircuits.

[13] R. H. Caverly and G. Hiller, "Distortion in p-i-n diode control circuits," *IEEE Transactions on Microwave Theory and Techniques*, vol. 35, no. 5, pp. 492–501, May 1987.

[14] R. H. Caverly and G. Hiller, "Distortion in microwave and rf switches by reverse biased pin diodes," in *IEEE MTT-S International Microwave Symposium Digest*, June 1989, pp. 1073–1076 vol.3.

[15] R. Caverley, "A nonlinear pin diode model for use in multi-diode microwave and rf communication circuit simulation," in *1988., IEEE International Symposium on Circuits and Systems*. IEEE, 1988, pp. 2295–2299.

[16] *D313060 ISOLATION 18dB*, DITOM.

[17] *ZN2PD-9G-S+ Combiner*, Minicircuits.

[18] *ZADC-10-63-S+ Directional Coupler*, Minicircuits.

[19] *R&S FSLSpectrum Analyzer Specifications*, RHODE&SCHWARZ, 03 2013, version 11.00.